

# Cattaneo-Christov Heat Flux Effect on Carreau Nanofluid over a Slippery Stretching Surface with Convective Boundary Condition

Toyin Wasiu Akaje, Olayemi Mukaila Alamu Yusuff, Bakai Ishola Olajuwon, Musiliu Tayo Raji, Olamilekan Fagbemiro

Department of Mathematics, Federal University of Agriculture, Abeokuta, Nigeria  
Email: akajewasiu@gmail.com

**How to cite this paper:** Akaje, T.W., Yusuff, O.M.A., Olajuwon, B.I., Raji, M.T. and Fagbemiro, O. (2025) Cattaneo-Christov Heat Flux Effect on Carreau Nanofluid over a Slippery Stretching Surface with Convective Boundary Condition. *Advances in Nanoparticles*, 14, 55-71.

<https://doi.org/10.4236/anp.2025.142004>

**Received:** March 26, 2025

**Accepted:** May 25, 2025

**Published:** May 28, 2025

Copyright © 2025 by author(s) and Scientific Research Publishing Inc.  
This work is licensed under the Creative Commons Attribution International License (CC BY 4.0).

<http://creativecommons.org/licenses/by/4.0/>



Open Access

## Abstract

This paper focuses on the effects of velocity and concentration slip with Cattaneo-Christov on magnetohydro dynamic viscoelastic material over a stretching surface with convective boundary conditions. The governing non-linear ordinary differential equations representation is fixed numerically by the weighted residual method (Galerkin method) The computed results are visualized graphically, and the validation of present solutions is reported by the comparative benchmark with already available results in a limiting sense. Our findings demonstrate that the opposite behaviour was noticed for the Brownian motion parameter and thermophoresis parameter as their values increases.

## Keywords

Carreau Nanofluid, Cattaneo-Christov Heat Flux, Convective Boundary Condition: Carreau Nanofluid

## 1. Introduction

Water, mineral, oil and ethylene are convectional heat transfer fluids that have poor heat transfer properties in comparison with those solids' materials in general. For enhancement of the heat transfer of fluid, Chio in 1995 [1] for the first time, introduced a nano-sized particle to a base fluid named nanofluid. Nanofluid consists of nano-sized particles (1 - 100 nm) such as metals, oxides, carbines or carbon nanotubes with base fluid. Choi *et al.* [2] showed that the thermal conductivity of the fluid upsurged approximately two times when a small amount (less than 1% by volume) of nanoparticle was added to a convenient heat transfer liquid. Bing

*et al.* [3] explored the radiation effect of MHD flow and heat transfer of Williamson nanofluid over a streaming set with Newtonian heating. Kumar *et al.* [4] investigated nonlinear thermal radiation and slip effect on Carreau nanofluid on stretched magnetic flow. Unsteady Carreau nanoparticle flow with conductivity was studied numerically by Irfanetal [5]. Fourier [6] introduced the heat conduction law to show the behaviour of heat transfer in various practical situations. The major issue reported was that the energy equation appears in a parabolic form, which means the system under consideration is instantly affected by initial disturbance. To control this, Fourier's law of several versions was introduced. Cattaneo [7] in his renowned article, includes the repose time for heat flux to Fourier's law. The time repose time for heat flux defines that once a temperature gradient is imposed, the time to establish a steady heat condition is known. Hayat *et al.* [8] use the homotopy analysis method to study Jeffrey fluid flow for Cattaneo-Christov heat flux in a three-dimensional rotating coordinate. They observed that the momentum boundary layer increases with a rise for a larger Deborah number while an upsurge in the Prandtl number and thermal relaxation time decrease in the temperature profile. Hayat *et al.* [9] explored MHD Oldroyd-B fluid in Cattaneo-Christov heat flux with homogeneous—heterogeneous reactions they deduced that the wall concentration decreases with increased values of the strengths of homogeneous—heterogeneous reactions parameter. Variable thermal conductivity fluid over a variable thickened effect on Cattaneo-Christov heat flux was examined by Hayat *et al.* [10] they ascertained that a higher thermal relaxation parameter decreases the temperature profile. Hayat *et al.* [11] analysed variable thickness impact on Cattaneo-Christov heat flux over a stretching sheet. They concluded that velocity and momentum boundary layer thickness reduces for larger values of Deborah number. Rotating flow and heat transfer of upper converted Maxwell fluid on Cattaneo-Christov heat flux studied by Mustafa [12]. He argued that there is an inverse relationship between Prandtl number and relaxation time of heat flux in the temperature region. Hen *et al.* [13] ascertained Cattaneo-Christov heat flux on coupled flow and heat in viscoelastic fluid. Khan *et al.* [14] examined three different types of nanofluid using Cattaneo-Christov heat flux model and OHAM. They reported that Cattaneo-Christov model of heat flux and the Fourier model have identical effects on the thermal relaxation parameter. The effect of Cattaneo-Christov heat flux on thermal instability in Brinkman porous media was examined by Haddad [15]. Khan *et al.* [16] inquired into the effect of heat on three-dimensional fluid and three-dimensional flow using Cattaneo-Christov heat flux model. Homogeneous-heterogeneous reactions and Cattaneo-Christov heat flux model effects on Darcy-Forchhermer flow was ascertained by Hayat *et al.* [17] Mahdy *et al.* [18], Mahatha *et al.* [19] and Uddin *et al.* [20] studied the slip effects on non-Newtonian fluid.

To the best of our knowledge, Cattaneo-Christov heat flux effect on Carreau nanofluid over a slippery stretching surface with convective boundary conditions has not been reported in the literature. The governing equations are solved via

Galerkin weighted residual method (GWRM). The graphs and tables are presented to illustrate and discuss the effects of various controlling flow parameters.

## 2. Mathematical Formulation

We considered the steady two-dimensional flow of an incompressible slip and Cattaneo-Christov heat flux effect on Carreau nanofluid over a slippery stretching surface with convective boundary conditions. The origin is at the slip and the lower wall is stationary while partial slip occurs at the upper wall. (see **Figure 1**). The  $x$ -axis is taken in the direction of the plate and the  $y$ -axis is normal to it. A transverse uniform magnetic field  $B_0$  is applied in the  $y$ -direction. On the stretching surface, the temperature and concentration of the fluid are represented with  $T$  and  $C$  respectively while  $T_\infty$  and  $C_\infty$  denotes the ambient temperature and concentration respectively. The extra stress tensor for Carreau fluid is given by the following expression:

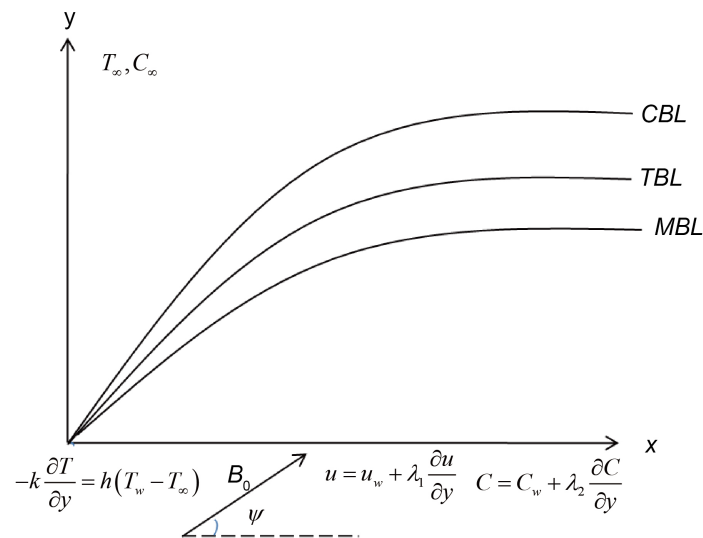


**Figure 1.** Flow geometry.

$$\tau = pI + \mu(\gamma)A_1$$

with

$$\mu(\gamma) = \mu_0 - (\mu_0 - \mu_\infty) \left(1 + (\Gamma\gamma)^2\right)^{\frac{n-1}{2}}$$

in which  $p$  is the pressure,  $I$  is the identity,  $\mu_0$  is the zero-shear rate,  $\mu_\infty$  is the infinity shear-rate viscosity,  $\Gamma$  is the material time constant and  $n$  is the power-law exponent.

The shear rate is expressed by

$$\gamma = \sqrt{\frac{1}{2}\Pi} = \sqrt{\frac{1}{2}\text{tr}(A_1^2)}$$

$$\dot{A}_1 = \nabla\hat{V} + (\nabla\hat{V})^T$$

where  $\Pi$  represents the second invariant strain rate tensor and  $\dot{A}_1$  stands for the Rivlin-Erickson tensor.

Using boundary layer approximation assumptions on the above, the basic conservation of mass, momentum, thermal energy and nanoparticles concentration equations are as follows:

$$\frac{\partial \tilde{u}}{\partial \tilde{x}} + \frac{\partial \tilde{v}}{\partial \tilde{y}} = 0 \tag{1}$$

$$\begin{aligned} & \tilde{u} \frac{\partial \tilde{u}}{\partial \tilde{x}} + \tilde{v} \frac{\partial \tilde{u}}{\partial \tilde{y}} \\ &= \nu \frac{\partial^2 \tilde{u}}{\partial \tilde{y}^2} \left[ 1 + \tilde{\Gamma}^2 \left( \frac{\partial \tilde{u}}{\partial \tilde{y}} \right)^2 \right]^{\frac{n-1}{2}} + \nu(n-1) \tilde{\Gamma}^2 \left( \frac{\partial \tilde{u}}{\partial \tilde{y}} \right)^2 \frac{\partial^2 \tilde{u}}{\partial \tilde{y}^2} \left[ 1 + \tilde{\Gamma}^2 \left( \frac{\partial \tilde{u}}{\partial \tilde{y}} \right)^2 \right]^{\frac{n-3}{2}} \\ &+ \frac{\sigma^* B_0^2}{\rho} \sin^2(\psi) \tilde{u} + g \tilde{\beta} (T - T_\infty) + g \tilde{\beta}^* (C - C_\infty) \end{aligned} \tag{2}$$

$$\begin{aligned} \tilde{u} \frac{\partial T}{\partial \tilde{x}} + \tilde{v} \frac{\partial T}{\partial \tilde{y}} &= \nu \frac{\partial^2 T}{\partial \tilde{y}^2} - \left\{ \tilde{u} \frac{\partial \tilde{u}}{\partial \tilde{x}} \frac{\partial T}{\partial \tilde{x}} + \tilde{v} \frac{\partial \tilde{v}}{\partial \tilde{y}} \frac{\partial T}{\partial \tilde{y}} + \tilde{u}^2 \frac{\partial^2 T}{\partial \tilde{x}^2} + \tilde{v}^2 \frac{\partial^2 T}{\partial \tilde{y}^2} + 2\tilde{u}\tilde{v} \frac{\partial^2 T}{\partial \tilde{x}\partial \tilde{y}} \right. \\ &\left. + \tilde{u} \frac{\partial \tilde{v}}{\partial \tilde{x}} \frac{\partial T}{\partial \tilde{y}} + \tilde{v} \frac{\partial \tilde{u}}{\partial \tilde{y}} \frac{\partial T}{\partial \tilde{x}} \right\} + \tau \left( D_B \frac{\partial T}{\partial \tilde{y}} \frac{\partial C}{\partial \tilde{y}} + \frac{D_T}{T_\infty} \left( \frac{\partial T}{\partial \tilde{y}} \right)^2 \right) \end{aligned} \tag{3}$$

$$\tilde{u} \frac{\partial C}{\partial \tilde{x}} + \tilde{v} \frac{\partial C}{\partial \tilde{y}} = D_B \frac{\partial^2 C}{\partial \tilde{y}^2} + \frac{D_T}{T_\infty} \frac{\partial^2 T}{\partial \tilde{y}^2} \tag{4}$$

The corresponding equations are subjected to the boundary conditions

$$\tilde{u} = \tilde{u}_w + \lambda_1 \frac{\partial \tilde{u}}{\partial \tilde{y}}, \tilde{v} = 0, -k \frac{\partial T}{\partial \tilde{y}} = h(T_\infty - T), C = C_w + \lambda_2 \frac{\partial C}{\partial \tilde{y}} \text{ at } \tilde{y} = 0 \tag{5}$$

$$\tilde{u} \rightarrow 0, T \rightarrow 0, C \rightarrow 0 \text{ as } \tilde{y} \rightarrow \infty \tag{6}$$

where  $\tilde{u}$  and  $\tilde{v}$  signifies along  $\tilde{x}$  and  $\tilde{y}$  direction respectively,  $B_0$  is the strength of the magnetic field,  $\tilde{\Gamma}$  is the material time constant,  $\nu = \frac{k}{\rho c_p}$  is the

thermal diffusivity such that  $k$  denotes the thermal conductivity and  $c_f$  is specific heat,  $T$  is the temperature distribution,  $C$  is the nanoparticles volume fraction, kinematic viscosity such that  $\mu_o$  stands for dynamic viscosity and  $\rho$  is the fluid density,  $\lambda_1$  and  $\lambda_2$  are the slip coefficient in velocity and concentration,  $D_B$  and  $D_T$  are the Brownian motion and thermophoresis diffusion coefficient.

Introducing the following similarity transformation

$$\eta = \sqrt{h}y, \psi = \sqrt{h\nu}xf(\eta), \theta(\eta) = \frac{T - T_\infty}{T_w - T_\infty}, \phi(\eta) = \frac{C - C_\infty}{C_w - C_\infty} \tag{7}$$

where  $h$  stands for  $\sqrt{\frac{a}{\nu}}$   $\eta$  is the similarity  $\psi$  is the stream function defined in the usual notation as  $u = \partial\psi/\partial y$  and  $v = -\partial\psi/\partial x$ .

Using similarity transformation quantities, the governing Equations (1)-(4) are transformed to the ordinary differential equation as follows:

$$(1+nWe f^{n2})(1+We f^{n2})^{\frac{n-3}{2}} f''' - f'^2 + ff'' + Gr\theta + Gc\phi - M^2 \sin^2(\psi) f' = 0 \quad (8)$$

$$\theta'' + Pr f \theta' - Pr \gamma (ff' \theta' + f^2 \theta'') + Pr (N_b \theta' \phi' + N_t \theta'^2) = 0 \quad (9)$$

$$\phi'' + Sc f \phi' + \frac{N_t}{N_b} \theta'' = 0 \quad (10)$$

The relevant boundary conditions are:

$$\begin{aligned} f = 0, \quad f' = 1 + \lambda_1 f'', \quad -\theta' = B_i [1 + \theta], \quad \phi = 1 + \lambda_2 \phi', \\ f'(\infty) \rightarrow 0, \quad \theta(\infty) \rightarrow 0, \quad \phi(\infty) \rightarrow 0 \end{aligned} \quad (11)$$

where primes denoted differentiation  $\eta$ . The governing dimensional parameters are defined as:

$$\begin{aligned} We = \frac{\ddot{\Gamma}^2 a^3 \tilde{x}^2}{\nu}, \quad M = \frac{\sigma B_0^2}{\rho a}, \quad Pr = \frac{\nu}{\alpha}, \quad N_b = \frac{D_B \lambda (C_w - C_\infty)}{\nu}, \\ N_t = \frac{D_T \lambda (T_w - T_\infty)}{\nu T_\infty}, \quad \gamma = a\tau, \quad Sc = \frac{\nu}{D_B}. \end{aligned} \quad (12)$$

where  $We$  is the local Weissenberg number,  $M$  is the magnetic parameter,  $Pr$  is the Prandtl number,  $N_b$  is the Brownian motion parameter,  $N_t$  is the thermophoresis parameter,  $\gamma$  is the non-dimensional thermal relaxation time,  $B_i$  is the Biot number and  $\lambda_1$  and  $\lambda_2$  represent slip coefficient in velocity and concentration respectively.

For the case of practical concern, the dimensionless physical quantities are the coefficient of skin friction and the Nusselt number and are expressed as

$$C_{fx} = \frac{\tau_w}{\rho U_w^2}, \quad Nu_x = -\frac{\tilde{x} q_w}{k(T_w - T_\infty)} \quad \text{and} \quad Sh_x = \frac{\tilde{x} q_m}{D_B(C_w - C_\infty)} \quad (13)$$

where

$$C_{fx} = \frac{\tau_w}{\rho U_w^2} \Big|_{y=0}, \quad Nu_x = -\frac{\tilde{x}}{T_w - T_\infty} \left( \frac{\partial T}{\partial \tilde{y}} \right)_{y=0} \quad (14)$$

$$q_w = k \left( \frac{\partial T}{\partial \tilde{y}} \right)_{\tilde{y}=0}, \quad \tau_w = \eta \frac{\partial \tilde{u}}{\partial \tilde{y}} \left[ 1 + \ddot{\Gamma}^2 \left( \frac{\partial \tilde{u}}{\partial \tilde{y}} \right)^2 \right]^{\frac{n-1}{2}} \Big|_{\tilde{y}=0}, \quad q_m = D_B \left( \frac{\partial C}{\partial \tilde{y}} \right)_{\tilde{y}=0} \quad (15)$$

With the help of Equation (7) and after simplification, the dimensionless form is reduced to

$$\begin{aligned} Re_x^{\frac{1}{2}} C_{fx} = f''(0) \left[ 1 + We^2 (f''(0))^2 \right]^{\frac{n-1}{2}}; \\ Re_x^{\frac{1}{2}} Nu_x = -\theta'(0); \quad Re_x^{-\frac{1}{2}} Sh_x = -\phi(0) \end{aligned} \quad (16)$$

where  $C_{fx}, Re_x, Nu_x, Sh_x$  are the skin friction, local Reynolds number, local Nusselt number and Sherwood number respectively.

### 3. Method of Solution

The method of weighted residual is engineering's tool for finding approximate

solutions for boundary value problems. The method is often applied in a complex situation of boundary value problems to get an appropriate numerical solution. Finlayson and Scriven [21] reviewed and examined various methods of weighted residual methods among which is the Galerkin weighted residual method (GWRM). Odejide and Aregbesola [22] use the weighted residual method to solve problems in the semi-infinite domain. Other contributors to the methods include Oderinu and Aregbesola [23], Aregbesola [24], Ghesemi *et al.* [25] and Francis [26].

The basic steps in Galerkin weighted residual methods (GWRM) are:

(i) Obtained an appropriate solution to the differential equation of the form:

$$L(u(y)) + f(y) = 0 \quad \text{on } \partial\Omega \quad (17)$$

where  $u(y)$  stand for the unknown dependent variable,  $f(y)$  stands for the independent function of the domain  $\partial\Omega$  and  $L$  stands for the differential operator.

(ii) The function  $\varphi$  (i.e. solution) is presumed to satisfy both the operator equation and the boundary conditions.

A trial function of the form

$$\varphi = \varphi_0 + \sum_{k=1}^n a_k \varphi_k \quad (18)$$

where  $a_k$  are constants to be determined? We select a trial function in a way that satisfied the boundary conditions including those at infinity. We include a function such as  $e^{-nx}$  for  $n > 0$  in the trial function which will make the trial function naturally satisfy the boundary condition.

(iii) Substituting Equation (17) into Equation (18) resorts to residual function  $R(y)$ . The main focus of weighted residual  $R(y)$  is to minimize the value in the domain  $\partial\Omega$  by integrating the product of the weighted function  $\varphi_k$  and residual function  $R(y)$  over the domain  $\partial\Omega$ .

$$\int_{\Omega} \varphi_k R(y) dy = 0, \quad k = 0, 1, \dots, n \quad (19)$$

(iv) We then applied the Gauss-Laguerre formula to get a system of algebraic equations by integrating each of the equations in Equation (19). The Gauss-Laguerre is used because of its usefulness in the boundary condition ranges of zero to infinity.

(v) The solutions are then sorted by solving the equations utilizing MATHEMATICA a computer-assisted symbolic package.

### Formula for Gauss-Laguerre

The formula Gauss-Laguerre takes the form

$$\int_0^{\infty} e^{-y} f(y) dy \approx \sum_{j=1}^n B_j f(y_j) \quad (20)$$

The argument  $y_j$  is the zeros of the  $n^{\text{th}}$  Laguerre polynomial

$$L_n(y) = e^y \frac{d^n}{dy^n} (e^{-y^n}) \quad (21)$$

and the coefficient  $B_j$  being

$$B_j = \frac{(n!)^2}{y_j [L'_n(y_j)]^2} \quad (22)$$

#### 4. Result Discussion

In this work, the impact of the Cattaneo-Christov heat flux effect on Carreau nanofluid over a slipper stretching surface with convective boundary conditions was examined. The surface variables on the velocity profile  $f'(\eta)$ , temperature profile  $\theta(\eta)$ , concentration profile  $\phi(\eta)$ , skin friction  $f''(\eta)$ , Nusselt number  $\theta'(\eta)$  and Sherwood number  $\phi'(\eta)$  inside the defined realm have been demonstrated through graphs and tables.

The present results align with earlier findings by Cortell [27] and Ramesh *et al.* [28] in the limiting case of no-slip and constant thermal flux. Furthermore, the observed behavior under increased magnetic field and thermal relaxation parameters correlates with Hayat *et al.* [9], who reported similar retardation effects in MHD viscoelastic flows.

Unless otherwise stated, default values (e.g.,  $Pr = 0.71$ ,  $Sc = 0.8$ ) were selected based on common physical properties of water-based nanofluids and prior literature [5] [29], and for numerical computation for the flow parameters are fixed as follows:

$$We = 0.3, \lambda_1 = 0.1, Pr = 0.71, Nt = 0.2, \lambda_2 = 0.1, Nb = 0.8, Gr = 0.31, \\ Sc = 0.8, \gamma = 0.1, B_i = 0.1, Gc = 0.3, M = 0.1, \psi = \pi/4.$$

To study the impact of non-dimensional velocity profiles  $f'$  subject to various involved parameters. **Figures 2-5** is sketched. **Figure 2** shows the graph of different values of the magnetic parameter  $M$  and non-dimensional thermal relaxation time  $\gamma$ . The velocity boundary layer reduces as the magnetic values parameter  $M$  increases which is justifiable because the magnetic field always causes a resistive force on fluid flow known as Lorentz force while enhancement in non-dimensional thermal relaxation time  $\gamma$  leads to a reduction in velocity profile and the momentum boundary layer thickness. From **Figure 3** we noticed that an upsurge in slip coefficient in velocity  $\lambda_1$  and slip coefficient in concentration  $\lambda_2$  lowered the fluid velocity. The effect of Grashof and modified Grashof parameters are shown in **Figure 4** and it is observed that the fluid flow rises with an enhancement of both Grashof and modified Grashof number hence velocity boundary thickness. The effects of parameters  $Pr$   $Sc$  are displayed in **Figure 5**, it was noticed that enhancement in  $Pr$  increases the momentum boundary thickness because increasing the Prandtl number corresponds to higher momentum diffusivity and thick boundary layer while the opposite occurs in Schmidt number  $Sc$ . Diminishing in Schmidt number occurs due to the dominance of mass diffusivity. The effect of the power-law index is sketched in **Figure 6**. An

increment in the value  $n$  strengthened the velocity and boundary layer thickness. Physically, an upsurge in the nonlinearity of the sheet reduces the opposite force and enhanced the velocity flow.

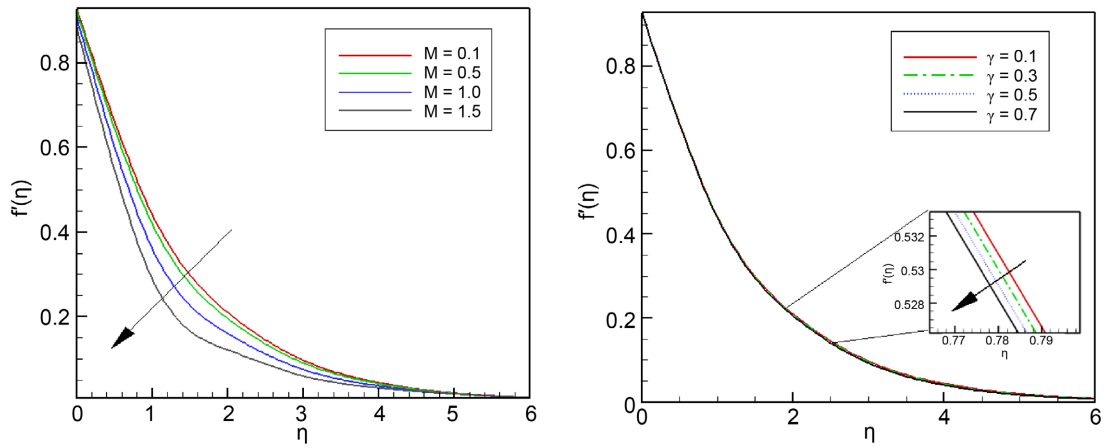


**Figure 2.** Impact of  $M$  and  $\gamma$  on  $f'(\eta)$ .

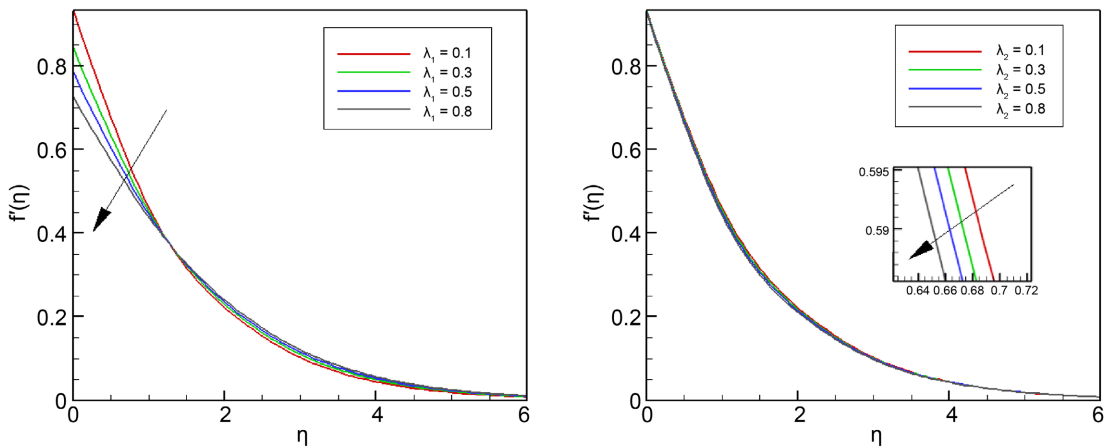


**Figure 3.** Impact of  $\lambda_1$  and  $\lambda_2$  on  $f'(\eta)$ .

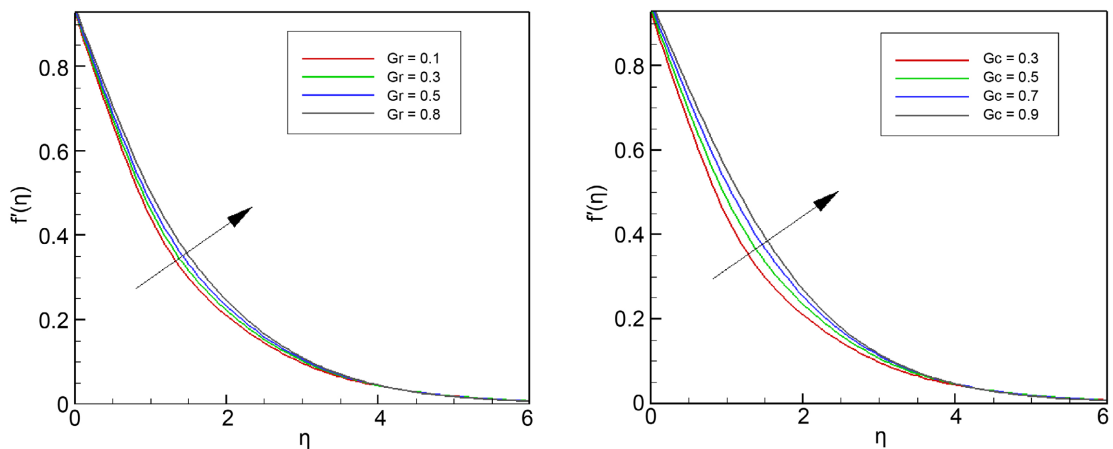


**Figure 4.** Impact of  $Gr$  and  $Gc$  on  $f'(\eta)$ .

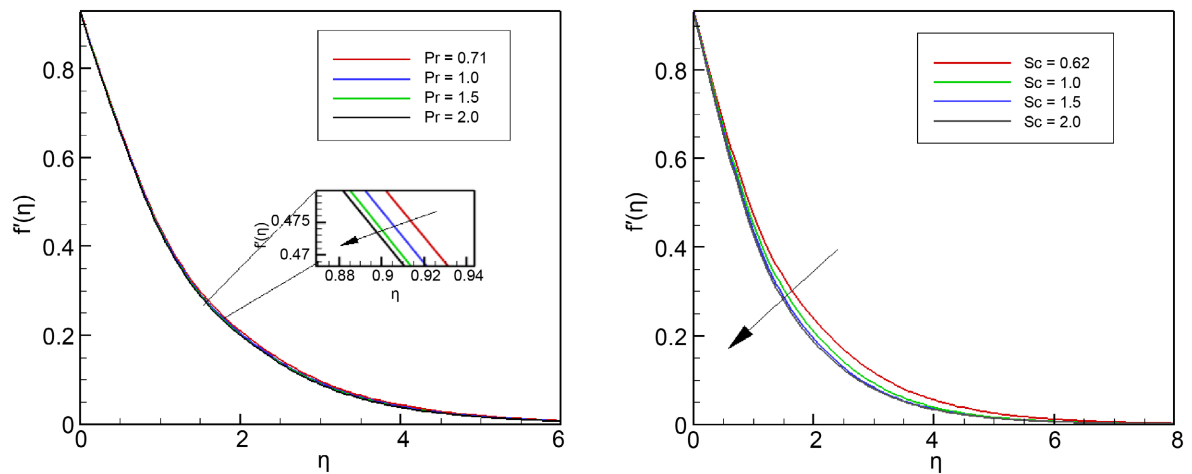


Figure 5. Impact of  $Pr$  and  $Sc$  on  $f'(\eta)$ .

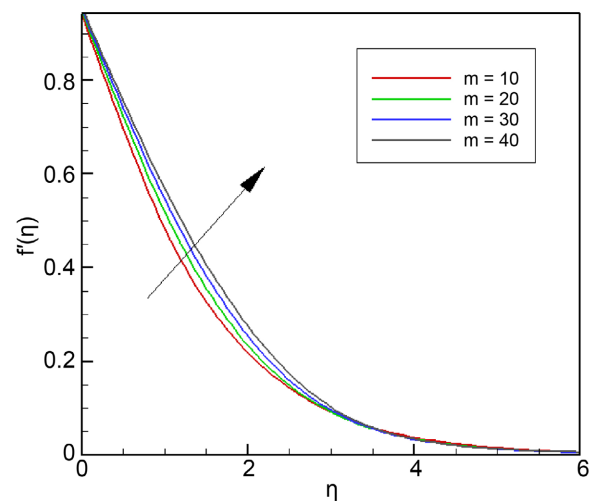


Figure 6. Impact of  $m$  on  $f'(\eta)$ .

To study the disparities in the temperature profile  $\theta(\eta)$  attributable to physical parameters. Figures 7-10 are sketched. Figure 7 is drawn to analyse the Brownian motion and thermophoresis parameters. These curves indicate that the thermal profile is enhanced as both material parameters  $Nb, Nt$  and are gradually increased. Different nanoparticles have different values  $Nb, Nt$  and hence an upsurge in the temperature profile. These two particles are used to control the heat transfer rate in nanofluids. The effect of the Prandtl number and Schmidt number on temperature profiles across the boundary layer is displayed graphically in Figure 8. It is clearly shown that the fluid temperature diminishes with an augment of  $Pr$ . It is due to an upsurge in Prandtl number  $Pr$  implies lower thermal diffusivity, reducing heat penetration into the fluid and thereby lowering the temperature profile. Hence the temperature profile and thermal boundary layer thickness decline while the thermal boundary layer thickness and absolute temperature increase with a rise in Schmidt number.

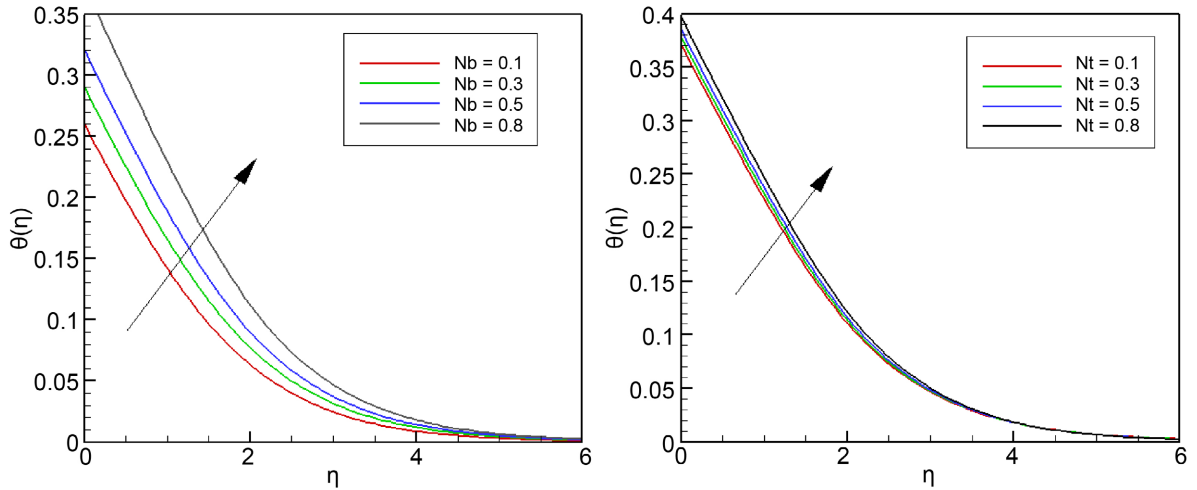


Figure 7. Impact of  $Nb$  and  $Nt$  on  $\theta(\eta)$ .

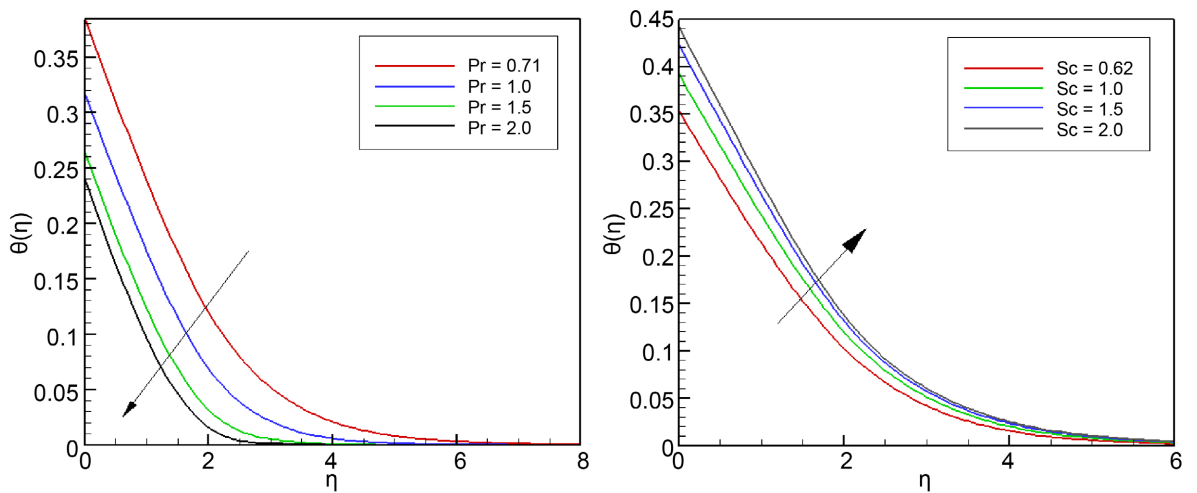


Figure 8. Impact of  $Pr$  and  $Sc$  on  $\theta(\eta)$ .

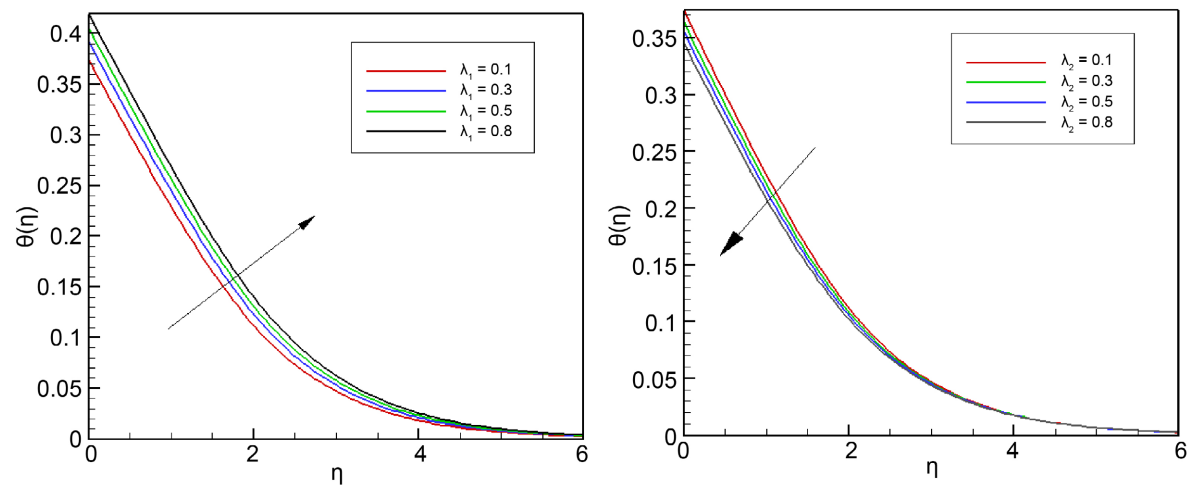
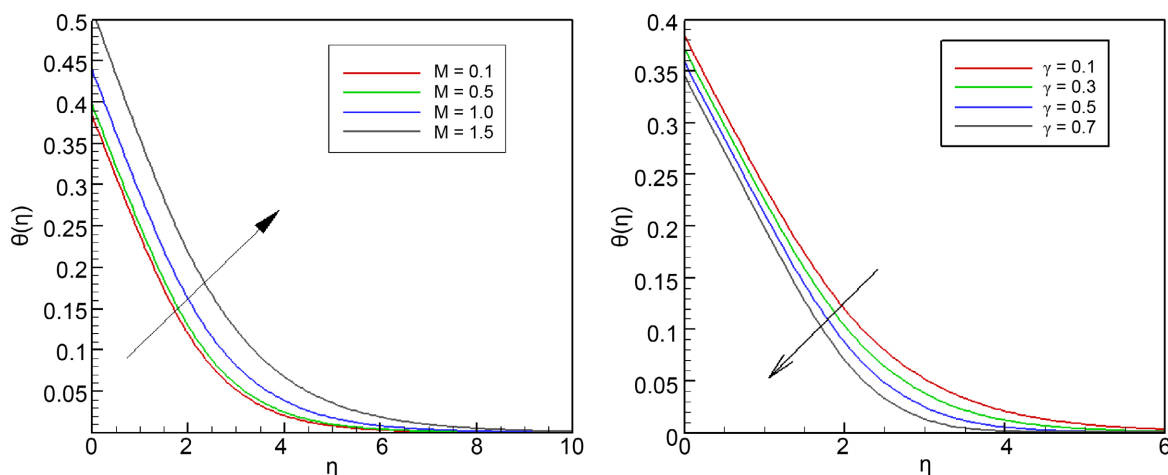


Figure 9. Impact of  $\lambda_1$  and  $\lambda_2$  on  $\theta(\eta)$ .



**Figure 10.** Impact of  $M$  and  $\gamma$  on  $\theta(\eta)$ .

**Figure 9** is prepared to look into the effect of slip coefficient in velocity and concentration parameters on the temperature profile  $\theta(\eta)$ . It is noticed that an increase in the slip coefficient in velocity results in an enhancement in the thermal profile and its boundary layer thickness, while an increase in slip coefficient in concentration weakens the temperature profile and results in thermal boundary layer thinning. **Figure 10** depicts the variation of the temperature profile due to the magnetic parameter  $M$  and the non-dimensional thermal relaxation time parameter  $\gamma$ . It is noticed from the figure that the thermal boundary layer thickness elevates with an upsurge in the values of  $M$  while the thermal boundary layer thickness of non-dimensional thermal relaxation time parameter  $\gamma$  decelerates as temperature increases. This is due to the drag force called Lorentz force presence in an electrically conducting magnetic field  $M$  which leads to the depreciation in velocity profile, extra work done in other to overcome this retardation causes thermal energy conversion which enhances the temperature of the fluid. While due to an increment in the thermal relaxation parameter, more time is required to transfer heat to its neighbouring particles. Higher values of thermal relaxation parameter material show a non-conducting behaviour which is responsible for decreasing the temperature profile.

The study of the influence of concentration profile  $\phi(\eta)$  on physical parameters is sketched in **Figures 11-14**. **Figure 11** explored the impact of the Brownian motion parameter  $Nb$  and the thermophoresis parameter. Enhancement in Brownian motion parameter physically associates with small-scale nanoparticle parameters as detailed by Rana *et al.* [30] hence the Brownian motion number diffusion is subdued therefore nanoparticle concentration boundary layer thickness is decreased. Heat transfer from the nanofluid regime to the plate surface is enhanced due to the thermophoresis migration of nanoparticles which considerably increases the nanoparticle concentration with greater  $Nt$  values. Identical remarks were made by Kumal *et al.* [4]. **Figure 12** illustrates the nanoparticle concentration for different velocity and concentration slips values the nanoparticle

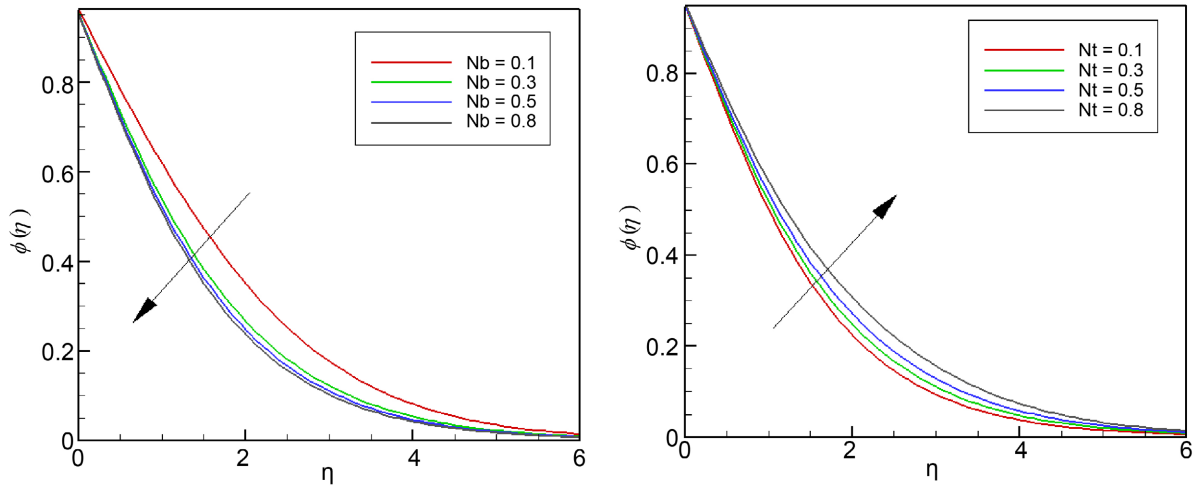


Figure 11. Impact of  $Nb$  and  $Nt$  on  $\phi(\eta)$ .

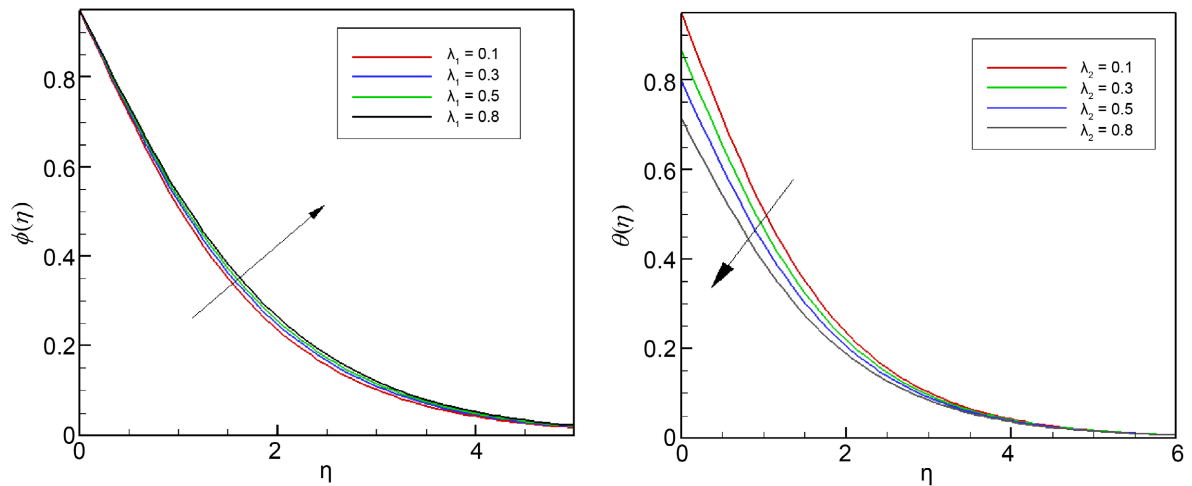


Figure 12. Impact of  $\lambda_1$  and  $\lambda_2$  on  $\phi(\eta)$ .

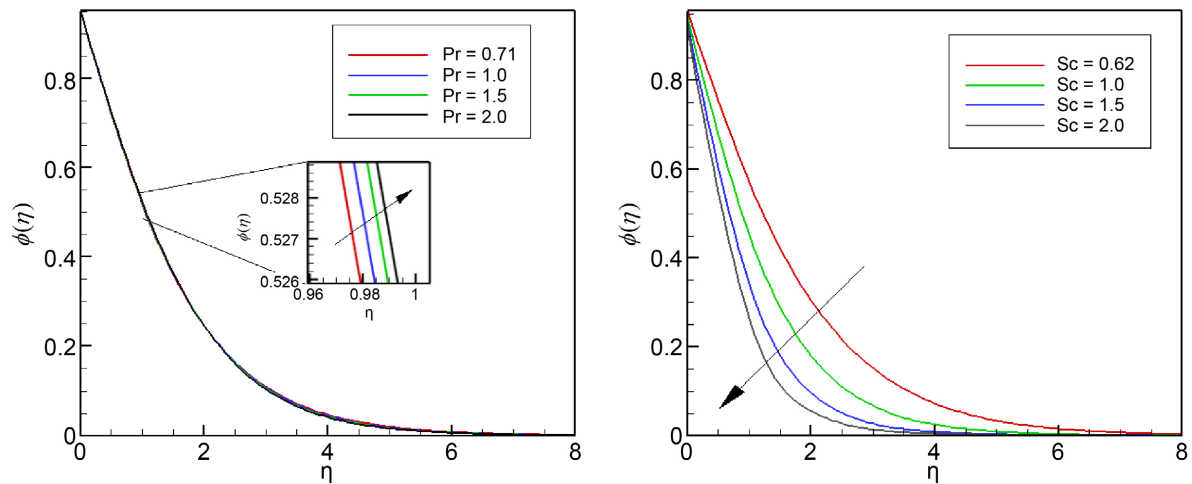
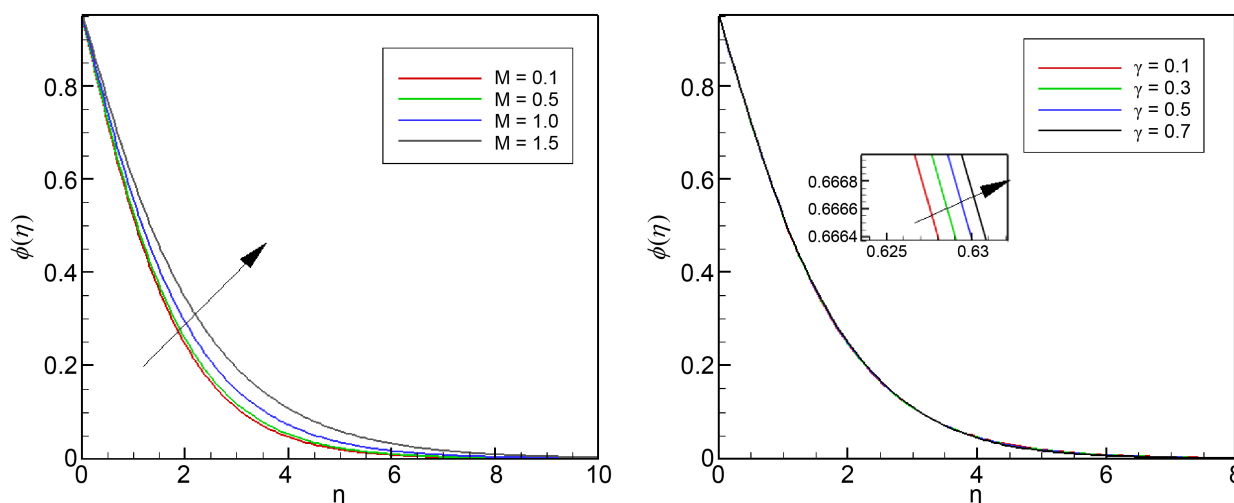


Figure 13. Impact of  $Pr$  and  $Sc$  on  $\phi(\eta)$ .



**Figure 14.** Impact of  $M$  and  $\gamma$  on  $\phi(\eta)$ .

concentration is enhanced with a greater velocity slip effect while the opposite behaviour is noticed for the concentration slip effect. The species boundary layer thickness is enlarged for velocity slip whereas the boundary layer thickness is reduced for concentration slip. Enhancement of the velocity slip factor leads to more transmission of heat to the fluid which energizes the boundary layer and hence increases the nanoparticle concentration. **Figure 13** depicts the effect of the Prandtl number and Schmidt number on nanoparticle concentration. The figure reveals that increasing the Prandtl number slightly elevates the nanoparticle magnitudes while the increase in Schmidt number diminishes the nanoparticle concentration. The Prandtl number indicates the ratio of momentum diffusion rate to thermal diffusion rate. An increase in the Prandtl number suppresses temperatures in the boundary layer. Prandtl number is inversely proportional to the thermal conductivity of the viscoelastic nanofluid which implies that a higher Prandtl number reduces thermal conductivity that inhibits thermal conduction heat transfer that cools the boundary layer which invariably leads to a slight increase in species nanoparticle concentration. Similar behaviour has been noted in studies on nanofluid flows. For example, in the work by Akaje and Olajuwon [31]. An increase in Schmidt's number means momentum diffusivity is greater than mass diffusivity. Since mass diffusivity depends on the nature of nanoparticle species in the base fluid, more repression in nanoparticle concentration results from a rise in Schmidt number. To analyse the influence of the magnetic parameter  $M$  and non-dimensional thermal relaxation time  $\gamma$  on concentration profile is sketched in **Figure 14**. An acclivity in the magnetic parameter  $M$  and non-dimensional thermal relaxation time  $\gamma$  causes an upsurge in the concentration boundary layer thickness.

The quantitative comparison with previously published papers is shown in **Table 1**. Several values of  $M$  for the skin friction coefficient  $-f''(0)$  are found to be tantamount to published papers. **Table 2** shows the variations of skin friction

**Table 1.** Comparison of several values  $M$  for the function  $-f''(0)$  when  $n=1$   $We = Gc = Gr = \lambda_1 = \lambda_2 = 0$   $Gr = 0$ ; and  $\psi = 90^\circ$  (absence of temperature and concentration).

$M$	Cortell [27]	Remesh <i>et al.</i> [28]	Kamar <i>et al.</i> [29]	Present
0	1.000	1.000	1.000	1.00000
0.2	1.095	1.095	1.095	1.09544
0.5	1.224	1.224	1.225	1.22474
1.0	1.414	1.414	1.414	1.41421
1.2	1.483	1.483	1.483	1.48324
1.5	1.581	1.581	1.581	1.58114
2.0	1.732	1.732	1.732	1.73205

**Table 2.** Comparison of skin friction coefficient, Nusselt number, and Sherwood number for different values of auxiliary parameters.

$M$	$\gamma Pr$	$Gr$	$Gc$	$Sc$	$Cf_x$	$Nu_x$	$Sh_x$
0.1	0.1	0.71	0.1	0.3	0.8	-0.707913	0.1384700.481043
0.5						-0.761127	0.1397830.470339
1.0						-0.913634	0.1439930.439856
1.5						-1.132869	0.1513630.397370
	0.3					-0.709335	0.1371960.480695
	0.5					-0.710730	0.1359040.135904
	0.7					-0.712072	0.1346130.480184
		1.0				-0.713945	0.1316920.479603
		1.5				-0.718491	0.1264310.478703
		2.0				-0.720578	0.1239940.478415
			0.3			-0.666172	0.1374520.489794
			0.5			-0.627592	0.1366070.497384
			0.8			-0.574169	0.1355590.507243
				0.5		-0.611534	0.1363640.499627
				0.7		-0.521591	0.1347700.515035
				0.9		-0.436515	0.1334880.528353
0.6							-0.6542980.1351220.410930
					0.78	-0.665143	0.1372450.482350
					0.96	-0.673476	0.1389360.546396

coefficient  $-f'(0)$  Nusselt number  $\theta(0)$  and Sherwood number  $\phi(0)$  for different values of governing parameters are calculated and summarized in **Table 2**. It is clear from the table that as the values of magnetic field  $M$ , non-dimensional thermal relaxation time  $\gamma$ , Prandtl number  $Pr$  and Schmidt number  $Sc$  increase, the values of skin friction coefficient increase while the Grashof  $Gr$  and modified Grashof parameters  $Gc$  dropped. It is also possible to see from the ta-

ble that enhancement in the values magnetic field  $M$ , Schmidt number  $Sc$ , non-dimensional thermal relaxation time  $\gamma$ , Prandtl number  $Pr$ , the Grashof  $Gr$  and modified Grashof parameters  $Gc$  give rises in Nusselt numbers for both magnetic field and Schmidt number and diminish for other parameters. As the values of the Grashof  $Gr$ , modified Grashof parameters  $Gc$  and Schmidt number  $Sc$  increase, the local Sherwood number  $-\phi'(\eta)$  increase while the opposite effect is observed for the magnetic field  $M$ , Prandtl number  $Pr$  and non-dimensional thermal relaxation time  $\gamma$ .

## 5. Conclusions

In this paper, the goal is to investigate the effects of velocity and concentration slip with Cattaneo-Christov on magnetohydrodynamic viscoelastic material over a stretching surface with convective boundary conditions. The method of weighted residual (Galerkin method.) is used to solve the governing nonlinear ordinary differential equations and results approved by numerical solution. The impact of various parameters on the non-dimensional velocity, temperature and concentration are investigated.

The summary of the results is as shown below:

- The velocity profile decreases with an increase in the magnetic parameter and non-dimensional thermal relaxation time.
- The thickness of the velocity boundary layer is enhanced as the value  $\lambda_1, \lambda_2$  increases.
- An enhancement in Magnetic number ends in a higher rate of skin friction drag coefficient.
- An increase in the slip coefficient in velocity results in an enhancement in the thermal profile while increasing the slip coefficient in concentration weakened the temperature profile.
- The concentration profiles slightly rise with an upsurge in the Prandtl number while an increase in the Schmidt number diminishes the nanoparticle concentration.
- An increase in non-dimensional thermal relaxation time leads to a diminishing in the Nusselt number
- The behaviour of velocity slip and concentration slip on the concentration profile is quite the opposite.

## Conflicts of Interest

The authors declare no conflicts of interest regarding the publication of this paper.

## References

- [1] Choi, S. (1995) Enhancing Thermal Conductivities of Fluids with Nanoparticle. In: Sisinger, D.A. and Wang, H.P., Eds., *Development and Application of Non-Newtonian Fluids*, American Institute of Mathematics Engineers, 99-105.
- [2] Choi, S.U.S., Zhang, Z.G., Yu, W., Lockwood, F.E. and Grulke, E.A. (2001) Anoma-

- lous Thermal Conductivity Enhancement in Nanotube Suspensions. *Applied Physics Letters*, **79**, 2252-2254. <https://doi.org/10.1063/1.1408272>
- [3] Bing, K.Y., Hussanan, A., Mohamed, M.K.A., Sarif, N.M., Ismail, Z. and Salleh, M.Z. (2017) Thermal Radiation Effect on MHD Flow and Heat Transfer of Williamson Nanofluids over a Stretching Sheet with Newtonian Heating. *AIP Conference Proceedings*, **1830**, Article 020022. <https://doi.org/10.1063/1.4980885>
- [4] Ganesh Kumar, K., Ramesh, G.K., Gireesha, B.J. and Rashad, A.M. (2019) On Stretched Magnetic Flow of Carreau Nanofluid with Slip Effects and Nonlinear Thermal Radiation. *Nonlinear Engineering*, **8**, 340-349. <https://doi.org/10.1515/nleng-2017-0120>
- [5] Irfan, M., Rafiq, K., Khan, W.A. and Khan, M. (2020) Numerical Analysis of Unsteady Carreau Nanofluid Flow with Variable Conductivity. *Applied Nanoscience*, **10**, 3075-3084. <https://doi.org/10.1007/s13204-020-01331-z>
- [6] Fourier, J.B.J. (1822) *Théorie Analytique de la Chaleur*. Cambridge University Press.
- [7] Cattaneo, C. (1948) Sulla conduzione del calore. *Attila Seminario Matematico e Fisicodella Università di Modena*, **3**, 83-101.
- [8] Hayat, T., Qayyum, S., Imtiaz, M. and Alsaedi, A. (2016) Three-Dimensional Rotating Flow of Jeffrey Fluid for Cattaneo-Christov Heat Flux Model. *AIP Advances*, **6**, Article 025012. <https://doi.org/10.1063/1.4942091>
- [9] Hayat, T., Imtiaz, M., Alsaedi, A. and Almezal, S. (2016) On Cattaneo-Christov Heat Flux in MHD Flow of Oldroyd-B Fluid with Homogeneous-Heterogeneous Reactions. *Journal of Magnetism and Magnetic Materials*, **401**, 296-303. <https://doi.org/10.1016/j.jmmm.2015.10.039>
- [10] Hayat, T., Farooq, M., Alsaedi, A. and Al-Solamy, F. (2015) Impact of Cattaneo-Christov Heat Flux in the Flow over a Stretching Sheet with Variable Thickness. *AIP Advances*, **5**, Article 287159. <https://doi.org/10.1063/1.4929523>
- [11] Hayat, T., Khan, M.I., Farooq, M., Alsaedi, A., Waqas, M. and Yasmeen, T. (2016) Impact of Cattaneo-Christov Heat Flux Model in Flow of Variable Thermal Conductivity Fluid over a Variable Thickened Surface. *International Journal of Heat and Mass Transfer*, **99**, 702-710. <https://doi.org/10.1016/j.ijheatmasstransfer.2016.04.016>
- [12] Mustafa, M. (2015) Cattaneo-Christov Heat Flux Model for Rotating Flow and Heat Transfer of Upper-Convected Maxwell Fluid. *AIP Advances*, **5**, Article 047109. <https://doi.org/10.1063/1.4917306>
- [13] Han, S., Zheng, L., Li, C. and Zhang, X. (2014) Coupled Flow and Heat Transfer in Viscoelastic Fluid with Cattaneo-Christov Heat Flux Model. *Applied Mathematics Letters*, **38**, 87-93. <https://doi.org/10.1016/j.aml.2014.07.013>
- [14] Khan, U., Ahmad, S., Hayyat, A., Khan, I., Nisar, K.S. and Baleanu, D. (2020) On the Cattaneo-Christov Heat Flux Model and OHAM Analysis for Three Different Types of Nanofluids. *Applied Sciences*, **10**, Article 886. <https://doi.org/10.3390/app10030886>
- [15] Haddad, S.A.M. (2014) Thermal Instability in Brinkman Porous Media with Cattaneo-Christov Heat Flux. *International Journal of Heat and Mass Transfer*, **68**, 659-668. <https://doi.org/10.1016/j.ijheatmasstransfer.2013.09.039>
- [16] Khan, M. and Khan, W.A. (2016) Three-dimensional Flow and Heat Transfer to Burgers Fluid Using Cattaneo-Christov Heat Flux Model. *Journal of Molecular Liquids*, **221**, 651-657. <https://doi.org/10.1016/j.molliq.2016.06.041>
- [17] Hayat, T., Haider, F., Muhammad, T. and Alsaedi, A. (2017) Darcy-Forchheimer Flow with Cattaneo-Christov Heat Flux and Homogeneous-Heterogeneous Reac-

- tions. *PLOS ONE*, **12**, e0174938. <https://doi.org/10.1371/journal.pone.0174938>
- [18] Mahdy, A. (2016) Unsteady MHD Slip Flow of a Non-Newtonian Casson Fluid Due to Stretching Sheet with Suction or Blowing Effect. *Journal of Applied Fluid Mechanics*, **9**, 785-793. <https://doi.org/10.18869/acadpub.jafm.68.225.24687>
- [19] Mahatha, B.K., Nandkeolyar, R., Nagaraju, G. and Das, M. (2015) MHD Stagnation Point Flow of a Nanofluid with Velocity Slip, Non-Linear Radiation and Newtonian Heating. *Procedia Engineering*, **127**, 1010-1017. <https://doi.org/10.1016/j.proeng.2015.11.450>
- [20] Uddin, M.J., Bég, O.A. and Ismail, A.I. (2015) Radiative Convective Nanofluid Flow Past a Stretching/Shrinking Sheet with Slip Effects. *Journal of Thermophysics and Heat Transfer*, **29**, 513-523. <https://doi.org/10.2514/1.t4372>
- [21] Finlayson, B.A. and Scriven, L.E. (1966) The Method of Weighted Residual Method—A Review. *Applied Mechanics Reviews*, **19**, 735-748.
- [22] Odejide, S. and Aregbesola, Y.A.S. (2011) Application of Method of Weighted Residuals to Problems with Semi-Infinite Domain. *Romanian Journal of Physics*, **1**, 14-24.
- [23] Oderinu, R.A. and Aregbesola, Y.A.S. (2012) The Weighted Residual Method in a Semi-Infinite Domain Using Un-Partitioned Methods. *International Journal of Applied Mathematics*, **25**, 25-31.
- [24] Aregbesola, Y.A.S. (2003) Numerical Solution of Bratu Problems Using of Weighted Residuals. *Electronic Journal of Southern African Mathematical Sciences Association*, **3**, 1-7.
- [25] Ghesemi, P.M., Abbasi, M. and Khaki, M. (2015) New Analytic Solution of MHD Fluid Flow of Fourth-Grade Fluid through the Channel with Slip Condition via Collocation Method. *International Journal of Advances in Applied Mathematics*, **2**, 87-94.
- [26] Scheid, F. (1964) Numerical Analysis, Schaum's Outline Series. McGraw-Hill Book Company.
- [27] Cortell, R. (2005) A Note on Magnetohydrodynamic Flow of a Power-Law Fluid over a Stretching Sheet. *Applied Mathematics and Computation*, **168**, 557-566. <https://doi.org/10.1016/j.amc.2004.09.046>
- [28] Ramesh, G.K., Gireesha, B.J. and Bagewadi, C.S. (2012) Stagnation Point Flow of a MHD Dusty Fluid towards a Stretching Sheet with Radiation. *Afrika Matematika*, **25**, 237-249. <https://doi.org/10.1007/s13370-012-0114-6>
- [29] Ganesh Kumar, K., Ramesh, G.K., Gireesha, B.J. and Rashad, A.M. (2019) On Stretched Magnetic Flow of Carreau Nanofluid with Slip Effects and Nonlinear Thermal Radiation. *Nonlinear Engineering*, **8**, 340-349. <https://doi.org/10.1515/nleng-2017-0120>
- [30] Rana, P., Bhargava, R., Bég, O.A. and Kadir, A. (2016) Finite Element Analysis of Viscoelastic Nanofluid Flow with Energy Dissipation and Internal Heat Source/Sink Effects. *International Journal of Applied and Computational Mathematics*, **3**, 1421-1447. <https://doi.org/10.1007/s40819-016-0184-5>
- [31] Akaje T.W., Olajuwon B.I., (2021) Impacts of Nonlinear Thermal Radiation on a Stagnation Point of an Aligned MHD Casson Nanofluid Flow with Thompson and Troian Slip Boundary Condition. *Journal of Advanced Research in Experimental Fluid Mechanics and Heat Transfer*, **6**, 1-15.